WEAK DISPERSION WAVE-FIELD SIMULATIONS: A PREDICTOR-CORRECTOR ALGORITHM FOR SOLVING ACOUSTIC AND ELASTIC WAVE EQUATIONS

NIAN WANG[1], DINGHUI YANG[1] and FAQI LIU[2]

[1] *Department of Mathematical Sciences, Tsinghua University, Beijing 100084, P.R. China.*
dhyang@math.tsinghua.edu.cn
[2] *Hess Corporation, One Allen Center, Houston, Texas 77002, U.S.A.*
fliu@hess.com

(Received October 3, 2011; revised version accepted February 19, 2012)

ABSTRACT

Wang, N., Yang, D. and Liu, F., 2012. Weak dispersion wave-field simulations: A predictor-corrector algorithm for solving acoustic and elastic wave equations. *Journal of Seismic Exploration*, 21: 125-152.

A new predictor-corrector algorithm (PCA) based on the implicit Runge-Kutta method is proposed to solve the acoustic and elastic wave equations. We transform the wave equation into a system of first-order partial differential equations (PDEs) with respect to time, convert the transformed wave equation into a semi-discrete ordinary differential equation (ODE) system by using the high-order interpolation method to approximate the spatial derivatives (Yang et al., 2003, 2007), and finally use the proposed PCA which is a time discretization method to solve the semi-discrete ODE system. We investigate the theoretical properties of the PCA such as its numerical convergence, stability criteria, and numerical dispersion for solving 1-D and 2-D scalar wave equations. The computational efficiency of the PCA in simulating acoustic wave fields is also investigated, and is compared with that of the staggered-grid method and the fourth-order Lax-Wendroff correction method (LWC). The effectiveness of the PCA is also demonstrated by its well matched waveforms to the analytic solution for modeling both acoustic and elastic models. Promising numerical simulation results indicate that the proposed PCA provides a useful method for the large-scale wave-field simulations because it can effectively suppress numerical dispersions even when coarse modeling grids are used or large velocity contrasts exist in geological models.

KEY WORDS: predictor-corrector algorithm, numerical dispersion, wave field simulation, implicit Runge-Kutta method.

0963-0651/12/$5.00

INTRODUCTION

Many numerical methods for solving acoustic and elastic wave equations have been developed and widely used in seismic modeling. The commonly used methods include finite difference methods (e.g., Virieux, 1984, 1986; Dablain, 1986; Fornberg, 1990; Lele, 1992; Takeuchi and Geller, 2000; Moczo et al., 2000; and many others), finite-element methods and adaptive finite-element methods (e.g., Turner et al., 1956 ; Whiteman, 1975; Johnson, 1990; Eriksson and Johnson, 1991, Yang et al., 2008), discontinuous Galerkin methods (e.g., Cockburn and Shu, 1989, 1998; Dumbser and Köser, 2006; Köser and Dumbser, 2006), pseudo-spectral method (PSM) (e.g., Kosloff and Baysal, 1982) and spectral element methods (e.g., Komatitsch and Vilotte, 1998; Komatitsch et al., 2000).

However, each method has its advantages and limitations. For example, the finite-difference (FD) methods, like the high-order FD (e.g., eighth-order method, Dablain, 1986) or compact FD methods, staggered-grid FD methods usually require less memory and can be easily implemented (e.g., Virieux, 1984, 1986; Levander, 1988; Fornberg, 1990; Luo et al., 1990; Moczo et al., 2000), but they often suffer from numerical dispersion when the computational grids are not fine enough or the sampling rate per wavelength is low. The finite-element method can be flexible in dealing with irregular computational region, but it requires large memory and computational time to solve linear algebraic equations. The pseudo-spectral method (PSM) only requires two grid points per wavelength to adequately represent the wavefront without apparent numerical dispersion (e.g., Kosloff and Baysal, 1982), but it still has numerical dispersion along time direction (Yang et al., 2006). In addition, the PSM can be time consuming due to the large number of Fourier transforms.

Effective suppression of the numerical dispersion is always attractive and has been widely studied by many researchers (e.g., Alford et al., 1974; Sei and Symes, 1994; Fei and Larner, 1995; Zhang et al., 1999; Yang et al., 2002). It has been well understood that a higher order FD scheme experiences less numerical dispersion for a given grid size and velocity model (Sei and Symes, 1994). However, the higher-order FD methods still have numerical dispersion (Dablain, 1986; Wang et al., 2002). Another way to deal with the numerical dispersion is to use the so-called flux-corrected transport (FCT) technique, but it can not fully recover the numerical dispersion when coarse spatial grids are used in the computation (Dablain, 1986, Fei and Larner, 1995; Zheng et al., 2006; Yang et al., 2006). Recently, the nearly analytic discrete (NAD) method and its optimal algorithms developed by Yang et al. (2003, 2006) are effective to reduce the numerical dispersion in solving both the acoustic wave-equation and the elastic wave-equation. More recently, different mixed methods combining the explicit or implicit Runge-Kutta methods with the NAD algorithm

have been developed (Yang et al., 2007, 2009). These methods use wave field displacement, particle-velocity and their gradient fields simultaneously to reconstruct wave displacement fields. As a result, they can keep more wave-field information because particle-velocity and their gradient fields include important wave-field information, further resulting in effectively suppressing the numerical dispersion caused by discretizing the wave equations.

Stability is one of the key factors for a numerical scheme, which is governed by the Courant number. Implicit methods are usually unconditionally stable. However, they need to solve many systems of large-scale linear algebraic equations, which can be computationally expensive and require large memory storage. A predictor-corrector method combined with an implicit scheme can inherit a good stability advantage without solving the large system of equations at each time step.

In this paper, we propose an explicit predictor-corrector algorithm (PCA) based on the implicit Runge-Kutta method (e.g., Hairer et al., 1993), which can effectively suppress the numerical dispersion. We first transform the wave equation into a system of first-order ordinary differential equations with respect to time t by using the NAD operators to approximate the spatial derivatives (Yang et al., 2003, 2007), and then use the PCA to solve the semi-discrete acoustic and elastic wave equations. Both theoretical analysis and numerical modeling for acoustic and elastic models show that the PCA can effectively suppress the numerical dispersion even when coarse grids are used, which indicates that it is computationally efficient and can be used in large scale wave-field simulations.

WAVE EQUATIONS

In a heterogeneous elastic medium, the linear elastic wave equation system can be written as

$$\rho(\partial^2\mathbf{u}/\partial t^2) = \nabla\cdot\boldsymbol{\sigma} + \mathbf{f} \ , \tag{1a}$$

$$\boldsymbol{\sigma} = \mathbf{C}:\boldsymbol{\varepsilon} \ , \tag{1b}$$

$$\boldsymbol{\varepsilon} = \tfrac{1}{2}[\nabla\mathbf{u} + (\nabla\mathbf{u})^T] \ , \tag{1c}$$

where eq. (1a) is the equation of motion, eq. (1b) is the constitutive equation, and eq. (1c) is the strain-displacement equation. The parameter ρ is the medium density, $\mathbf{u} = (u_1,u_2,u_3)^T$ is the displacement vector, $\boldsymbol{\sigma}$ and $\boldsymbol{\varepsilon}$ are respectively the Cauchy stress tensor and the infinitesimal strain tensor, $\mathbf{C}$ is the fourth-order stiffness tensor, and $\mathbf{f} = (f_1,f_2,f_3)^T$ is the external force.

By substituting eqs. (1b) and (1c) into eq. (1a), we can get the displacement equation as follows,

$$\rho(\partial^2\mathbf{u}/\partial t^2) = \mathbf{D}\cdot\mathbf{u} + \mathbf{f} \ , \tag{2}$$

where $\mathbf{D}$ is the second-order partial differential operator. For the 2D isotropic elastic medium, we have

$$\sigma_{i,j} = \lambda\delta_{i,j}\sum_{k=1}^{3}\varepsilon_{k,k} + 2\mu\varepsilon_{i,j} \ , \quad i,j \in \{1,2,3\}$$

where λ and μ are Lamé constants, then the corresponding matrix $\mathbf{D}$ in eq. (2) is

$$\begin{bmatrix} (\lambda+2\mu)\dfrac{\partial^2}{\partial x^2}+\mu\dfrac{\partial^2}{\partial z^2} & 0 & (\lambda+\mu)\dfrac{\partial^2}{\partial x\partial z} \\ 0 & \mu\left(\dfrac{\partial^2}{\partial x^2}+\dfrac{\partial^2}{\partial z^2}\right) & 0 \\ (\lambda+\mu)\dfrac{\partial^2}{\partial x\partial z} & 0 & \mu\dfrac{\partial^2}{\partial x^2}+(\lambda+2\mu)\dfrac{\partial^2}{\partial z^2} \end{bmatrix}.$$

In the following, we transform eq. (2) into a system of ordinary differential equations (Yang et al., 2007, 2009). Define $\mathbf{w} = \partial\mathbf{u}/\partial t = (\partial u_1/\partial t, \partial u_2/\partial t, \partial u_3/\partial t)^T$, then eq. (2) can be written as

$$\begin{aligned} &\partial\mathbf{u}/\partial t = \mathbf{w} \ , \\ &\partial\mathbf{w}/\partial t = (1/\rho)\mathbf{D}\cdot\mathbf{u} + (1/\rho)\mathbf{f} \ . \end{aligned} \tag{3}$$

Eq. (3) can be written in a compact vector form as

$$\partial\mathbf{v}/\partial t = \mathbf{L}\cdot\mathbf{v} + \mathbf{g} \ , \tag{4}$$

where

$$\mathbf{L} = \begin{bmatrix} \mathbf{0} & \mathbf{I} \\ (1/\rho)\mathbf{D} & \mathbf{0} \end{bmatrix} , \quad \mathbf{g} = \begin{pmatrix} \mathbf{0} \\ (1/\rho)\mathbf{f} \end{pmatrix} \text{ and } \quad \mathbf{v} = (\mathbf{u},\mathbf{w})^T \ .$$

The PCA uses wave field displacement, particle-velocity and their gradient fields to approximate the high-order spatial derivatives (Yang et al., 2003, 2007). Define vectors $\tilde{\mathbf{v}} = (\mathbf{v},\mathbf{v}_x,\mathbf{v}_z)^T$, $\tilde{\mathbf{f}} = (\mathbf{g},\mathbf{0},\mathbf{0})^T$ and $\tilde{\mathbf{L}} = diag(\mathbf{L},\mathbf{L},\mathbf{L})$ in which $\mathbf{v}_x = \partial\mathbf{v}/\partial x$ and $\mathbf{v}_z = \partial\mathbf{v}/\partial z$, from eq. (4) we get the following first order ODE system

$$\partial\tilde{\mathbf{v}}/\partial t = \tilde{\mathbf{L}}\cdot\tilde{\mathbf{v}} + \tilde{\mathbf{f}} \quad . \tag{5}$$

PREDICTOR-CORRECTOR ALGORITHM

To solve the wave equation (5), we approximate the spatial derivatives included in its right-hand side by the NAD operator (Kondoh et al., 1994; Yang et al., 2003; Yang et al., 2007), and get a system of semi-discrete ordinary differential equations. Then we solve the semi-discrete ODE system by a predictor-corrector algorithm (PCA) based on the implicit Runge-Kutta method. The NAD operator uses not only the values of the displacement **u** and particle velocity **w** at the mesh point (i,j) and its neighboring grid points, but also the values of their gradient fields to approximate the high-order spatial derivatives in eq. (5). The detailed computational formulae are listed in Appendix A.

To solve the semi-discrete ODE system (5), we use the diagonal implicit Runge-Kutta method (e.g., Hairer et al., 1993)

$$\tilde{\mathbf{v}}^{n+1}_{i,j} = \tilde{\mathbf{v}}^{n}_{i,j} + (\Delta t/2)(\mathbf{k}^{n}_{i,j} + \tilde{\mathbf{k}}^{n}_{i,j}) \quad , \tag{6}$$

$$\mathbf{k}^{n}_{i,j} = \tilde{\mathbf{L}}(\tilde{\mathbf{v}}^{n}_{i,j} + r\Delta t\mathbf{k}^{n}_{i,j}) + \tilde{\mathbf{f}}_{i,j}(t_n + r\Delta t) \quad , \tag{7}$$

$$\tilde{\mathbf{k}}^{n}_{i,j} = \tilde{\mathbf{L}}[\tilde{\mathbf{v}}^{n}_{i,j} + (1 - 2r)\Delta t\mathbf{k}^{n}_{i,j} + r\Delta t\tilde{\mathbf{k}}^{n}_{i,j}] + \tilde{\mathbf{f}}_{i,j}[t_n + (1 - r)\Delta t] \quad , \tag{8}$$

where $r = (1/2) - (\sqrt{3}/6)$.

To obtain the value of $\tilde{\mathbf{v}}^{n+1}$ which is the value of at the (n+1)-th time step in eq. (6), we need to compute $\mathbf{k}^{n}_{i,j}$ and $\tilde{\mathbf{k}}^{n}_{i,j}$ from eqs. (7) and (8), which are respectively the approximations to the slopes of the unknown function $\tilde{\mathbf{v}}$ at time $t_n + r\Delta t$ and $t_n + (1 - r)\Delta t$. However, direct computation of $\mathbf{k}^{n}_{i,j}$ and $\tilde{\mathbf{k}}^{n}_{i,j}$ needs to solve two systems of linear algebraic equations at each time step, which can be computationally intensive. In the following section, we propose a predictor-corrector method to improve the efficiency in computing $\mathbf{k}^{n}_{i,j}$ and $\tilde{\mathbf{k}}^{n}_{i,j}$. This method is similar to the strong stability-preserving method developed by Shu and Osher (1988) and Shu (1988).

The predictor and corrector steps for explicitly computing $\mathbf{k}^{n}_{i,j}$ in eq. (7) are described in detail as follows. We first compute the predictor by

$$\mathbf{k}^{n}_{i,j}{}^{(1)} = \tilde{\mathbf{L}}\tilde{\mathbf{v}}^{n}_{i,j} \quad . \tag{9}$$

The corrector is then computed in the following two steps,

$$\mathbf{k}_{i,j}^{n\,(2)} = \mathbf{k}_{i,j}^{n\,(1)} + r\Delta t\tilde{\mathbf{L}}\mathbf{k}_{i,j}^{n} = \tilde{\mathbf{L}}\tilde{\mathbf{v}}_{i,j}^{n} + r\Delta t\tilde{\mathbf{L}}^2\tilde{\mathbf{v}}_{i,j}^{n} \quad , \tag{10}$$

$$\begin{aligned}\mathbf{k}_{i,j}^{n} &= \mathbf{k}_{i,j}^{n\,(2)} + r\Delta t\tilde{\mathbf{L}}\mathbf{k}_{i,j}^{n\,(2)} + \tilde{\mathbf{f}}_{i,j}(t_n + r\Delta t) \\ &= \tilde{\mathbf{L}}\tilde{\mathbf{v}}_{i,j}^{n} + 2r\Delta t\tilde{\mathbf{L}}^2\tilde{\mathbf{v}}_{i,j}^{n} + (r\Delta t)^2\tilde{\mathbf{L}}^3\tilde{\mathbf{v}}_{i,j}^{n} + \tilde{\mathbf{f}}_{i,j}(t_n + r\Delta t) \quad ,\end{aligned} \tag{11}$$

where the second-order operator $\tilde{\mathbf{L}}^2$ can be obtained from $\tilde{\mathbf{L}}$ as follows

$$\begin{aligned}\tilde{\mathbf{L}}^2 &= \mathrm{Diag}(\mathbf{L}^2,\mathbf{L}^2,\mathbf{L}^2) \\ &= \mathrm{Diag}[(1/\rho)\mathbf{D},(1/\rho)\mathbf{D},(1/\rho)\mathbf{D},(1/\rho)\mathbf{D},(1/\rho)\mathbf{D},(1/\rho)\mathbf{D}] \quad .\end{aligned} \tag{12}$$

Similarly, we can explicitly compute $\tilde{\mathbf{k}}_{i,j}^{n}$ in eq. (8) by using a similar predictor-corrector approach

$$\begin{aligned}\tilde{\mathbf{k}}_{i,j}^{n} &= \tilde{\mathbf{k}}_{i,j}^{n\,(2)} + r\Delta t\tilde{\mathbf{L}}\tilde{\mathbf{k}}_{i,j}^{n\,(2)} + \tilde{\mathbf{f}}_{i,j}[t_n + (1-r)\Delta t] \\ &= \tilde{\mathbf{L}}\tilde{\mathbf{w}}_{i,j}^{n} + 2r\Delta t\tilde{\mathbf{L}}^2\tilde{\mathbf{w}}_{i,j}^{n} + (r\Delta t)^2\tilde{\mathbf{L}}^3\tilde{\mathbf{w}}_{i,j}^{n} + \tilde{\mathbf{f}}_{i,j}[t_n + (1-r)\Delta t] \quad ,\end{aligned} \tag{13}$$

where $\tilde{\mathbf{k}}_{i,j}^{n\,(2)} = \tilde{\mathbf{L}}\tilde{\mathbf{w}}_{i,j}^{n} + r\Delta t\tilde{\mathbf{L}}^2\tilde{\mathbf{w}}_{i,j}^{n}$, $\tilde{\mathbf{w}}_{i,j}^{n} = \tilde{\mathbf{v}}_{i,j}^{n} + (1-2r)\Delta t\mathbf{k}_{i,j}^{n}$.

Combining eq. (6) with eqs. (9)-(13), we obtain the explicit PCA.

For practical applications, the implementation of the PCA is divided into the following major steps:

1. Compute $\mathbf{k}_{i,j}^{n}$ using eqs. (9)-(11).

   (a) Compute $\tilde{\mathbf{L}}\tilde{\mathbf{v}}_{i,j}^{n}$ and $\tilde{\mathbf{L}}^2\tilde{\mathbf{v}}_{i,j}^{n}$ using eq. (12) and (A-1) to (A-7), and then substituting them into eq. (10) to obtain $\mathbf{k}_{i,j}^{n\,(2)}$;

   (b) Compute $\tilde{\mathbf{L}}\mathbf{k}_{i,j}^{n\,(2)}$ using the formulae (A-1) to (A-7) and the result $\mathbf{k}_{i,j}^{n\,(2)}$ in step (a);

   (c) Substitute these results obtained in steps (a) and (b) into eq. (11) to obtain $\mathbf{k}_{i,j}^{n}$.

2. Compute $\tilde{\mathbf{k}}_{i,j}^{n}$ following the similar steps as in computing $\mathbf{k}_{i,j}^{n}$. The only difference is that, the vectors $\tilde{\mathbf{v}}_{i,j}^{n}$ and $\mathbf{k}_{i,j}^{n\,(2)}$ in eqs. (10) and (11) are replaced by the vectors $\tilde{\mathbf{w}}_{i,j}^{n}$ and $\tilde{\mathbf{k}}_{i,j}^{n\,(2)}$, respectively.

3. Substitute the results $\mathbf{k}_{i,j}^{n}$ and $\tilde{\mathbf{k}}_{i,j}^{n}$ into eq. (6) to obtain the values of $\tilde{\mathbf{v}}_{i,j}^{n+1}$ at the (n+1)-th time step.

THEORETICAL PROPERTIES OF THE PCA

Theoretical error

Using the Taylor series expansion, the error of the interpolation formulae for spatial derivatives listed in Appendix A can be verified to be $O(\Delta x^4 + \Delta z^4)$. The temporal error, however, is $O(\Delta t^2)$ because we use the third-order implicit Runge-Kutta method and the predictor-corrector method. Therefore, the PCA has a fourth-order accuracy in space and second-order accuracy in time.

Convergence rate

In this subsection, we use the following 2D initial value problem for the acoustic wave equation to demonstrate the numerical accuracy and convergence of the PCA,

$$(\partial^2 u/\partial x^2) + (\partial^2 u/\partial z^2) = (1/c^2)(\partial^2 u/\partial t^2) \quad , \tag{14a}$$

$$u(0,x,z) = \cos[-(2\pi f_0/c)x\cos\theta_0 - (2\pi f_0/c)z\sin\theta_0] \quad , \tag{14b}$$

$$\partial u(0,x,z)/\partial t = -2\pi f_0 \sin[-(2\pi f_0/c)x\cos\theta_0 - (2\pi f_0/c)z\sin\theta_0] \quad , \tag{14c}$$

where c is the velocity of the medium, θ_0 is the incident angle at time $t = 0$, f_0 is the frequency. It is known that this initial problem has an exact solution as follows,

$$u(t,x,z) = \cos\{2\pi f_0[t - (x/c)\cos\theta_0 - (z/c)\sin\theta_0]\} \quad . \tag{15}$$

In the numerical experiment, the computational domain is: $0 < x \leq 20$ km and $0 < z \leq 20$ km; the frequency $f_0 = 10$ Hz, the velocity $c = 4000$ m/s, $\theta_0 = \pi/4$ and the maximum propagation time is $T = 1$ s. The error of the numerical solution u_h with respect to the exact solution is measured in the L^∞-norm (e.g., Dumbser and Käser, 2006), i.e.,

$$E_{L^\infty} = \| u_h - u \| = h^2 \max_{i,j} | u^n_{i,j} - u(t_n,x_i,z_j) | \quad . \tag{16}$$

The convergence rate is defined by (e.g., Dumbser and Köser, 2006)

$$O_{L^\infty} = \log(E^n_{L^\infty}/E^{n-1}_{L^\infty})/\log(h^n/h^{n-1}) \quad . \tag{17}$$

where $u^n_{i,j}$ and $u(t_n,x_i,z_j)$ are respectively the numerical solution and the analytical solution for the n-th time step of the initial problem [see eq. (14)], h^n is the spatial step for time t_n.

Table 1 shows the convergence rate O_{L^∞} of the PCA for different spatial and temporal grid sizes with the same Courant number $\alpha = 0.1$ ($\alpha = c\Delta t/\Delta x$), where its first column is the spatial increment, the second column is the error E_{L^∞}, and the third column shows the convergence rate of the PCA. From this table, we can conclude that the numerical convergence rate of the PCA is about 3, which is a combined effect of time and spatial accuracy. In addition, the convergence rates do not vary considerably as the spatial grid size increases, which demonstrates that the PCA is a robust numerical scheme.

Table 1. Convergence rates of the PCA.

Δx	E_{L^∞}	O_{L^∞}
8.00E-2	1.4938E-002	-
4.00E-2	2.3584E-003	2.6632
2.00E-2	3.3487E-004	2.8161
1.00E-2	4.4533E-005	2.9106

Stability criteria

It is well known that the temporal and spatial grid sizes relative to a given velocity must satisfy certain relationship to keep the numerical scheme stable. Using Fourier analysis methods (e.g., Richtmeyer and Morton, 1967; Yang et al., 2006), we derive the following stability criteria of the PCA for the 1D acoustic case (see Appendix B for details)

$$c_0(\Delta t/\Delta x) \leq \alpha_{max} \approx 0.626 \ , \tag{18}$$

or

$$\Delta t \leq \alpha_{max}(\Delta x/c_0) \approx 0.626(\Delta x/c_0) \ , \tag{19}$$

where c_0 denotes the wave velocity, Δt and Δx are the time and spatial increments, respectively.

Similarly, for the 2D acoustic case, we can obtain the following stability condition of the PCA,

$$\Delta t \leq \alpha_{max}(\Delta x/c_0) \approx 0.556(\Delta x/c_0) \ . \tag{20}$$

Here we assume $\Delta x = \Delta z = h$.

For an anisotropic heterogeneous elastic medium, the Courant number α_{max} can not be determined exactly because the velocity of the wave varies at different wavelength-scale or in different directions when it propagates through the computational region. But it can be approximately obtained by using a local homogeneous method. Our conjecture is that the stability criteria given in eqs. (19) and (20) are still valid in a heterogeneous medium if we use the maximum velocity c_0.

NUMERICAL DISPERSION AND EFFICIENCY

To investigate the effectiveness of the PCA in suppressing the numerical dispersion, we derive its numerical dispersion relations for both 1D and 2D cases and compare them against those of the high-order LWC methods (e.g., Dablain, 1986) and the fourth order staggered-grid FD method (SG) (e.g., Luo et al., 1990; Moczo et al., 2000). Detailed derivation can be found in Appendix C.

Fig. 1 shows the numerical dispersion curves of the PCA (Fig. 1a), eighth-order LWC (Fig. 1b), and the tenth-order LWC method (Fig. 1c) corresponding to different Courant numbers for solving the 1D acoustic wave equation, from which we can see that the PCA and the high-order LWC methods have the same variation pattern as the Courant number increases. In other words, for a small Courant number, the numerical velocity is usually smaller than the real one, especially in the high frequency range, whereas the numerical velocity becomes larger when the Courant number is relatively large. However, when the Courant number is less than 0.5, the numerical dispersion error of the PCA is smaller than those of both the eighth-order and tenth-order LWC methods. For example, when Courant number is equal to 0.3, the maximal deviation of the numerical velocity of the PCA from the real one is about 5%, whereas the corresponding errors of the high-order LWC methods such as eighth-order and tenth-order LWC methods are about 15% for the same case.

Fig. 2 is the 2D numerical dispersion curves of the PCA (Fig. 2a, and Fig. 2c) and the fourth-order staggered-grid FD method (SG) (Fig. 2b and Fig. 2d) for the acoustic wave equation at different propagation angles with respect to the x-axis for the Courant number $\alpha = 0.1$ (Fig. 2a and Fig. 2b) and $\alpha = 0.4$ (Fig. 2c and Fig. 2d), where the four lines are corresponding to the propagation angles being $\upsilon = 0°, 15°, 30°, 45°$, respectively. It is shown that the maximal deviation of the numerical velocity from the exact one is no greater than 10% for the PCA, while it is about 25% for the SG method under the same Courant number. In addition, the numerical dispersion error of the PCA does not show significant variation for different propagation angles, which means that the PCA has little numerical anisotropy for the 2D case.

We now investigate the numerical dispersion and computation efficiency of the PCA in wave-field simulation. Here, we consider the following 2D acoustic wave equation

$$(\partial^2 u/\partial t^2) = c_0^2[(\partial^2 u/\partial x^2) + (\partial^2 u/\partial z^2)] + f \ , \tag{21}$$

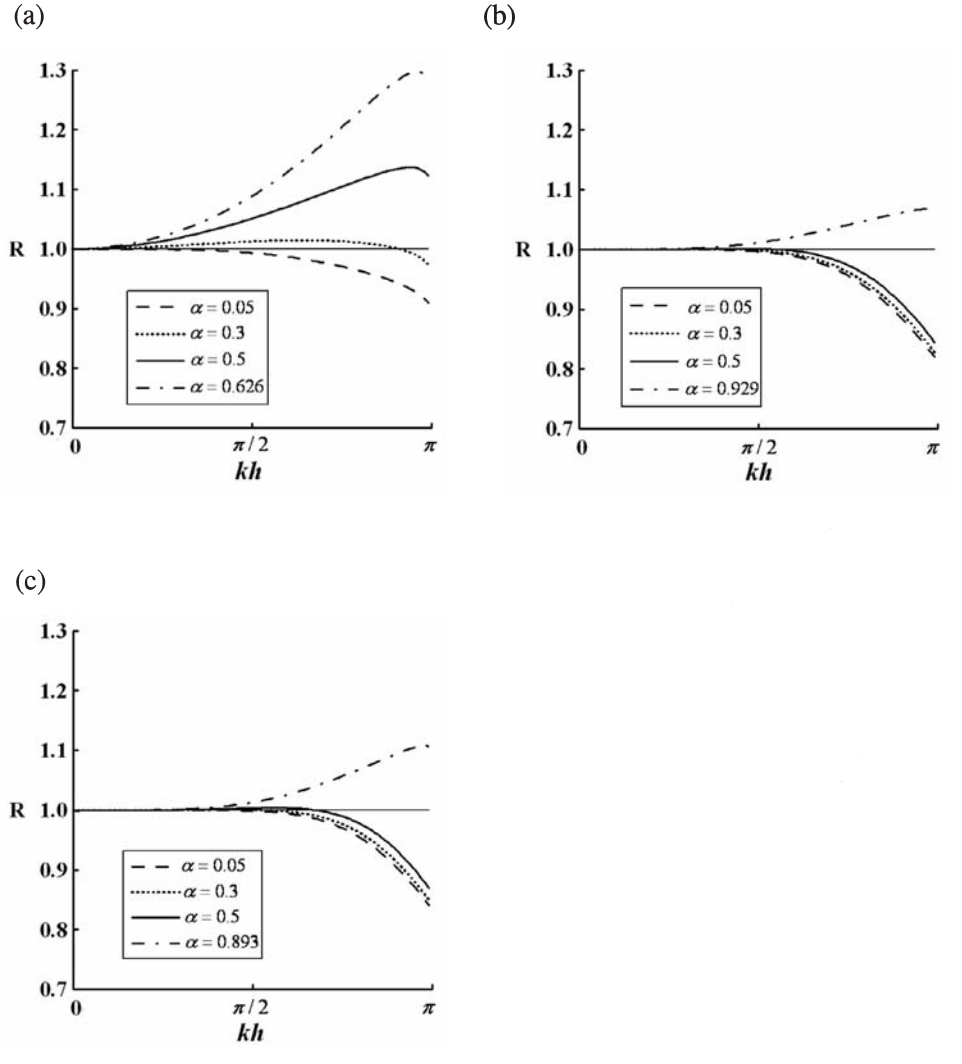

Fig. 1. The ratio R of the numerical velocity to the phase velocity versus wave-number respectively for (a) the PCA, (b) the eighth-order LWC method, and (c) the tenth-order LWC method, where four lines correspond to $\alpha = 0.05$, 0.3, 0.5, and α_{max}, respectively.

where the force source located at the center of the computational domain, is a Ricker wavelet defined as $f = \sin(2\pi f_0)\exp(-4\pi^2 f_0^2 t^2/16)$ (Zahradnik et al., 1993) with the peak frequency $f_0 = 20$ Hz. The velocity is $c_0 = 4000$ m/s and the computation domain is $0 < x \leq 15$ km and $0 < z \leq 15$ km.

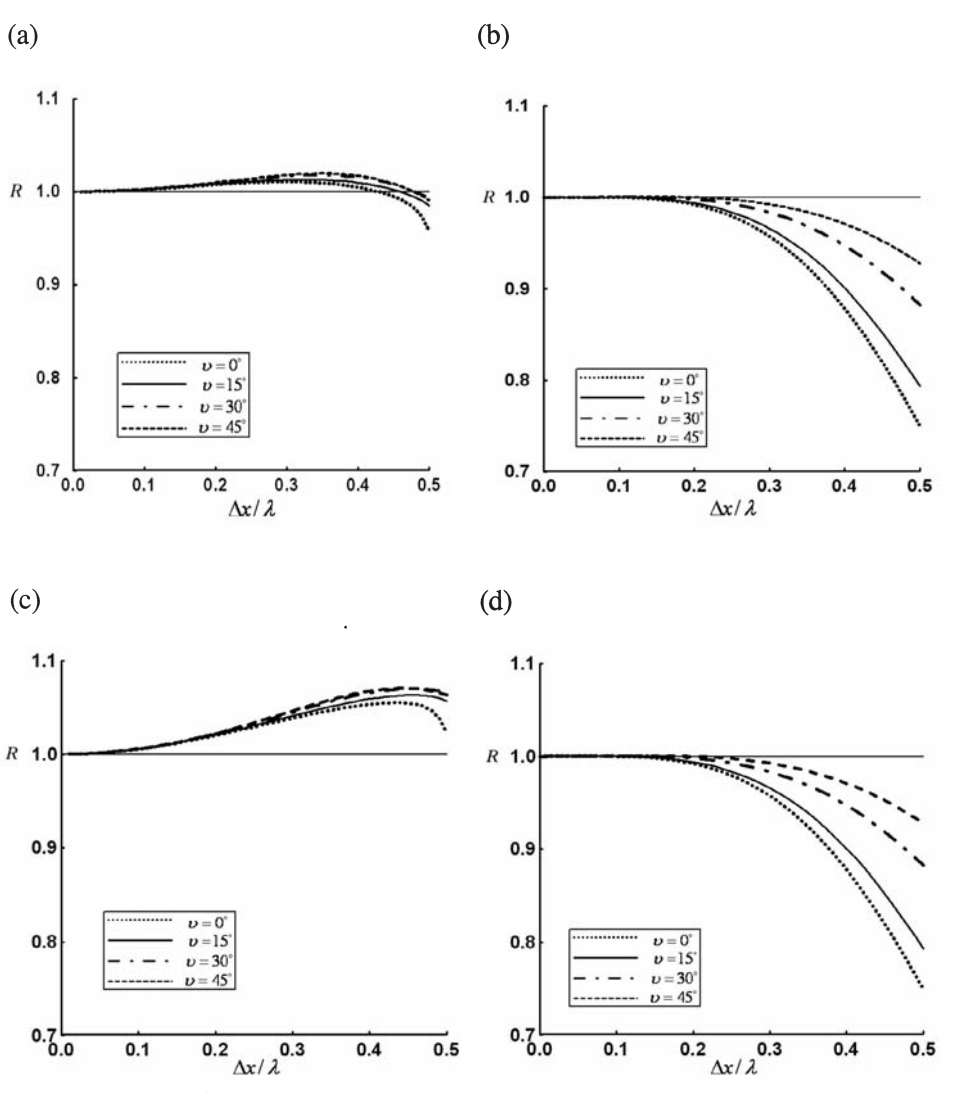

Fig. 2. The ratio R of the numerical velocity to the phase velocity versus $\Delta x/\lambda$ (the wavelength λ), generated by the PCA (a) and the fourth-order SG (b) under the Courant number $\alpha = 0.1$, and the PCA (c) and the fourth-order SG (d) under the Courant number of $\alpha = 0.4$, for different propagation angles with respect to the x-axis, where four lines correspond to $\upsilon = 0°, 15°, 30°, 45°$, respectively.

Fig. 3 shows the wave-field snapshots at t = 1.6 s computed on a very coarse grid ($\Delta x = \Delta z = 60$ m) which means about 3.3 grid points per shortest wavelength, generated respectively by the PCA, the fourth-order LWC and the fourth-order staggered-grid (SG) FD method. Fig. 4 shows the wave-field snapshots generated by the fourth-order LWC with $\Delta x = \Delta z = 10$ m and the fourth-order staggered-grid (SG) FD method with even a finer grid of $\Delta x = \Delta z = 8$ m, respectively, at the same time step under the same Courant number to effectively suppress the numerical dispersion. We can see that the wave fronts shown in Fig. 3, simulated by the three methods are nearly identical. However, the result generated by the PCA (Fig. 3a) shows no visible numerical dispersion even for such a coarse grid of 60 m (about 3.3 points in the shortest wavelength), whereas the results of both the fourth-order LWC and staggered-grid FD methods are severely dispersed (see Figs. 3b and 3c).

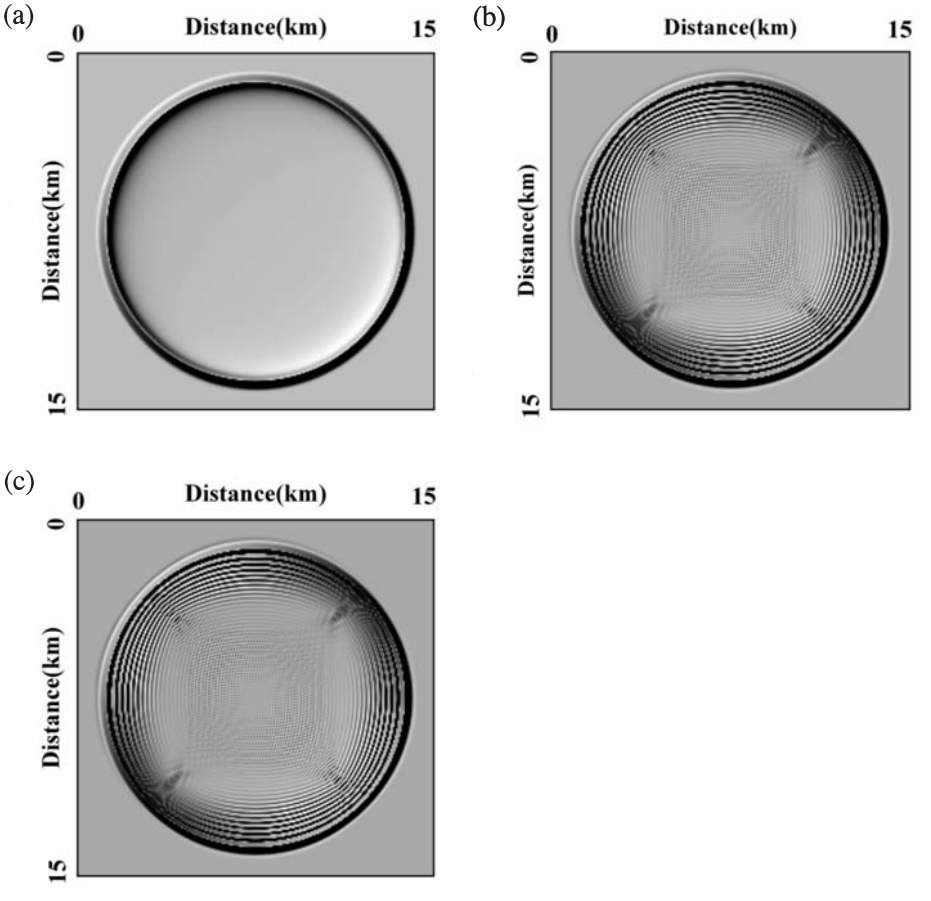

Fig. 3. Snapshots of seismic wave fields at time 1.6 sec on the coarse grid ($\Delta x = \Delta z = 60$ m), generated by the fourth-order LWC (a), the fourth-order SG (b), and the PCA (c), respectively.

Comparison between Fig. 3(a) and Fig. 4 demonstrates that the PCA can produce the same accurate wave field snapshot with no visible numerical dispersion on a much coarser grid as those of the fourth-order LWC and the fourth-order staggered-grid (SG) FD method on significantly finer grids. But their computational costs are quite different: it took the PCA about 11.7 min to compute Fig. 3(a), but the fourth-order LWC method and the fourth-order staggered-grid (SG) FD method took about 438.2 minutes and 195.3 minutes to generate Figs. 4(a) and 4(b), respectively. It means that, to achieve the same accuracy, the PCA is about 37 times faster than the fourth-order LWC and 17 times faster than the fourth-order staggered-grid (SG) FD method.

Even though the PCA needs 24 arrays to store the wave fields and their gradients, the fourth-order LWC and the staggered-grid (SG) method, on the other hand, need only 3 and 5 arrays, respectively, to store the displacements to produce the same accurate results, the coarser grids for the PCA results in a significant saving in memory usage. Fig. 3(a) was computed on a 251 $\times$ 251 grid, while Figs. 4(a) and 4(b) were computed on a grid of 1501 $\times$ 1501 for the fourth-order LWC and 1875 $\times$ 1875 for the fourth-order staggered-grid (SG) FD method, respectively. Therefore, the PCA takes only about 22% and 9% of the memory that required by the fourth-order LWC and the fourth-order staggered-grid (SG) FD method, respectively.

To show the accuracy of the PCA in wave-field simulation, we compare its waveform with the analytical solution computed using the Cagniard-de Hoop method (Aki and Richards, 1980). In this experiment, the computational domain is $0 \leq x \leq 10$ km and $0 \leq z \leq 10$ km, the acoustic velocity $c = 4000$ m/s,

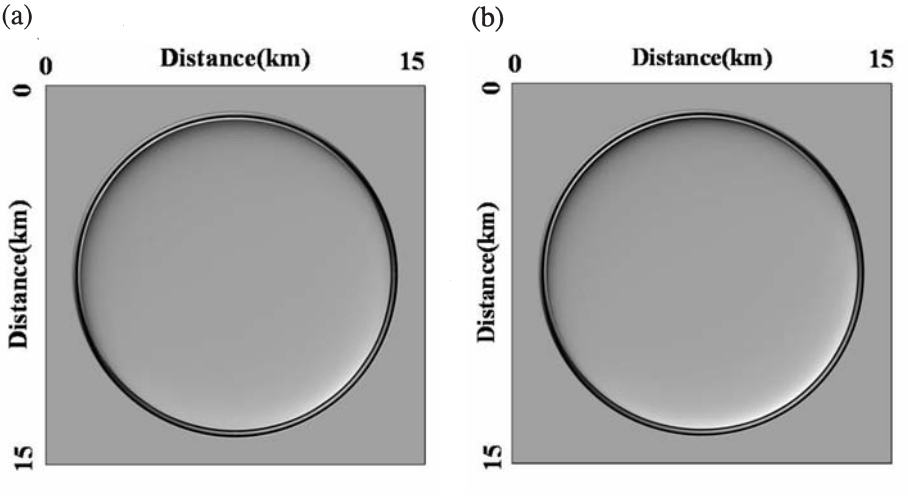

Fig. 4. Snapshots of seismic wave fields at time 1.6 sec on a fine grid, generated by (a) the fourth-order LWC ($\Delta x = \Delta z = 10$ m) and (b) the fourth-order SG ($\Delta x = \Delta z = 8$ m).

the spatial increment $\Delta x = \Delta z = 20$ m. The source is located at the center S (5 km, 5 km) and defined as

$$f = -5.76f_0^2[1 - 16(0.6f_0t - 1)^2]\exp[-8(0.6f_0t - 1)^2] \quad . \tag{22}$$

Fig. 5 shows the comparison of waveforms for receiver at R(4.2 km, 5 km) generated respectively by using the PCA, fourth-order LWC, and the staggered-grid (SG) method with a central frequency $f_0 = 50$ Hz against the analytical result denoted by the solid line, from which we see that the PCA result (Fig. 5a) matches well with the seismogram calculated by the Cagniard-de Hoop method, but Figs. 5(b) and 5(c) show that the fourth-order LWC and the SG methods have serious numerical dispersion.

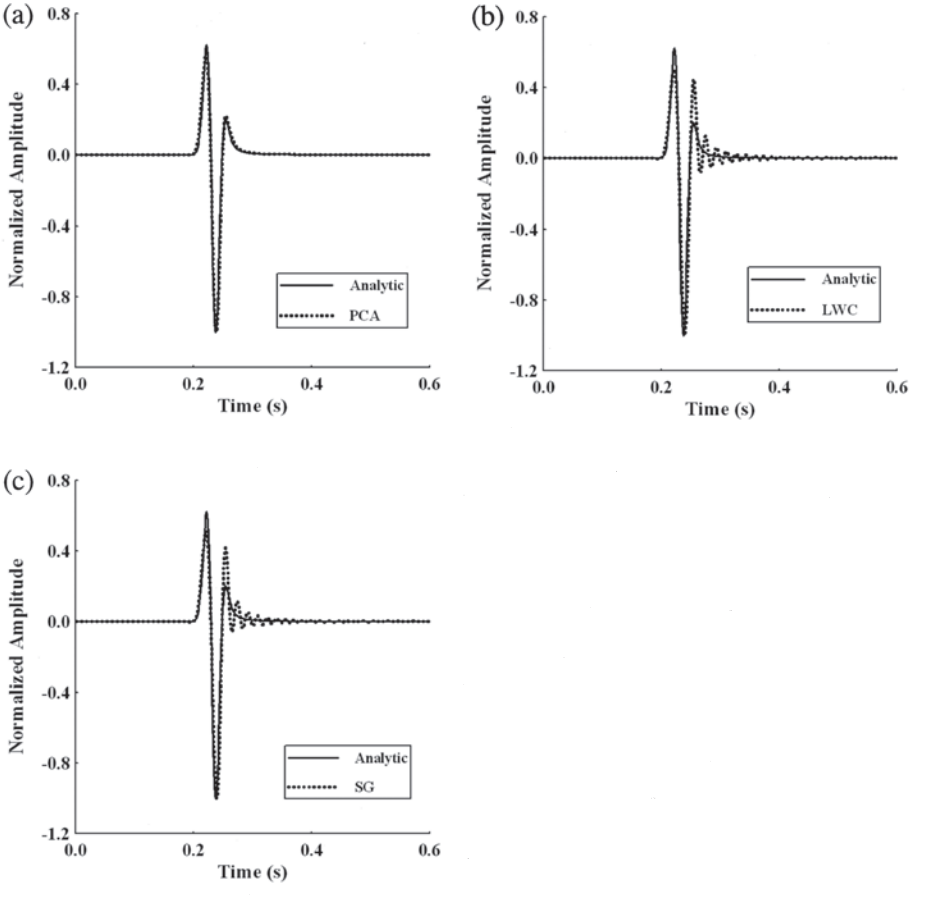

Fig. 5. Comparison of waveforms for the high frequency 50 Hz with the analytical solution for the acoustic case, generated by (a) the PCA, (b) the fourth-order LWC, and (c) the fourth-order SG, where the solid and dashed lines denote the analytical solution and the numerical solution, respectively.

Fig. 6 shows the comparison of waveforms generated by the PCA and the analytical solution with central source frequency $f_0 = 50$ Hz for receivers at R(4 km, 4 km) that is about 17 wavelength away from the source (Fig. 6a) and at R(3.5 km, 3.5 km) that is about 26 wavelength away from the source (Fig. 6b). Both figures show good match between the simulation result of PCA and the Cagniard-de Hoop method, which demonstrates the PCA is accurate for far-field computation.

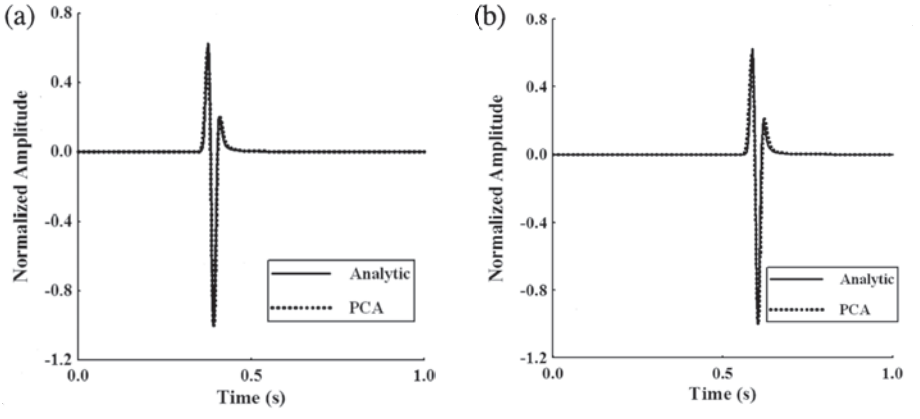

Fig. 6. Comparison of waveforms generated by the PCA and the analytical solution for the high frequency 50 Hz for the acoustic case, recorded at receiver R(4 km, 4 km) (a) and receiver R(3.5 km, 3.5 km) (b).

Fig. 7 shows the PCA results computed at frequencies as high as 70 Hz (Fig. 7a) and 90 Hz (Fig. 7b) for a fixed spatial grid size of 20 m. No dispersive noise can be noticeable even for the peak frequency of 90 Hz, these clean waveforms confirm the effective simulation of PCA.

To test the effectiveness of the PCA in numerical simulation for more complicated models, we chose a two-layer acoustic model which has a velocity of 2 km/s in the upper layer and 4 km/s in the lower layer. The computational region is $0 < x \leq 4$ km and $0 < z \leq 4$ km, and the depth of the horizontal interface is at $z = 2.2$ km. The source is the same one used in the above acoustic model with a peak frequency of $f_0 = 40$ Hz, and it is located at the coordinate (2 km, 1.6 km). The spatial increment is 8 m, and the time step is $\Delta t = 1 \times 10^{-4}$ s. Fig. 8 is the comparison of waveforms computed by the PCA and the analytic solution at the receiver R(1.6 km, 1.2 km), from which we can see that the two waveforms match with each other quite well, which illustrates that the PCA is accurate for modeling the layered acoustic medium which has large velocity contrast between adjacent layers.

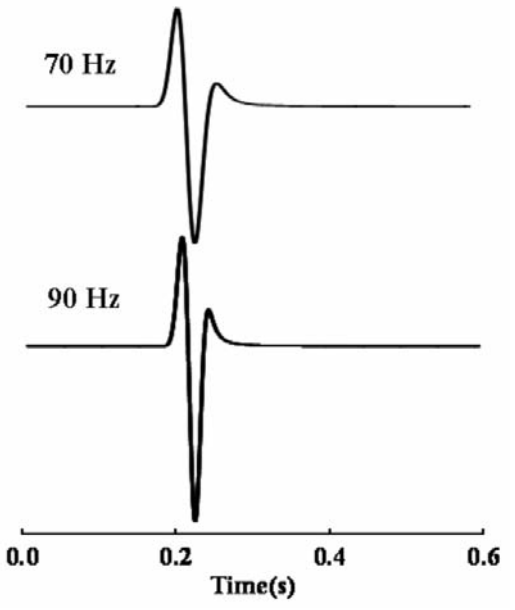

Fig. 7. Waveforms for different peak frequencies of (a) 70 Hz and (b) 90 Hz, computed by PCA for a fixed spatial increment $\Delta x = \Delta z = 20$ m for the acoustic model.

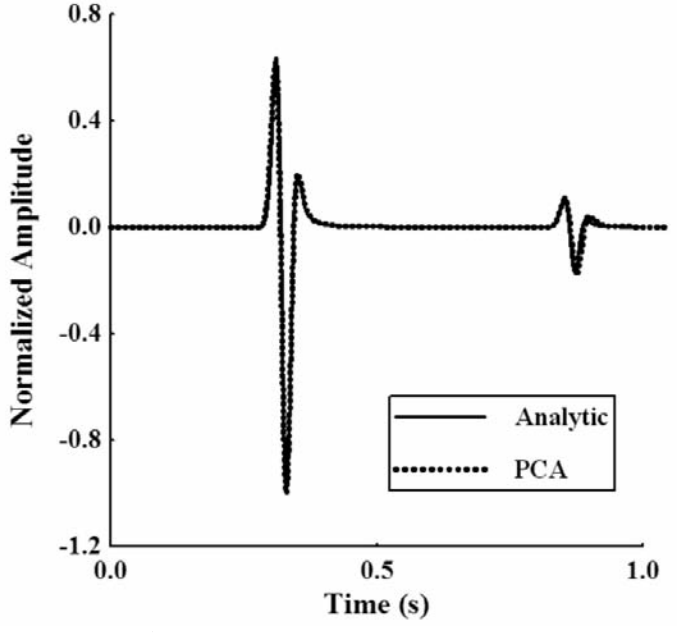

Fig. 8. Comparison of waveforms generated by the PCA for the high frequency ($f_0 = 40$ Hz) on the spatial grid ($\Delta x = \Delta z = 8$ m) with the analytical solution for the two-layer acoustic model.

We also test the validity of the PCA in the elastic case by comparing its waveforms with the analytic solution. The P- and S-wave velocities are respectively $4\sqrt{3}$ km/s and 4 km/s, and the density is $\rho = 1$ g/cm^3. The computation region is $0 \leq x \leq 16$ km and $0 \leq z \leq 16$ km, the three components of the source vector are also given by eq. (22) with a peak frequency $f_0 = 40$ Hz, and the source is located at the center of the region with the coordinate S(8 km, 8 km). The spatial increment is 10 m, and the time step is $\Delta t = 1 \times 10^{-4}$ s. Fig. 9 shows the waveforms comparison between the PCA and the analytic solution at time T = 1.2 s for the receiver at R(6 km, 6 km), which is about 28 wavelength away from the source location. From the nice match of the waveforms for both the direct P- and S-waves, we conclude that the PCA is also accurate for modeling the elastic case.

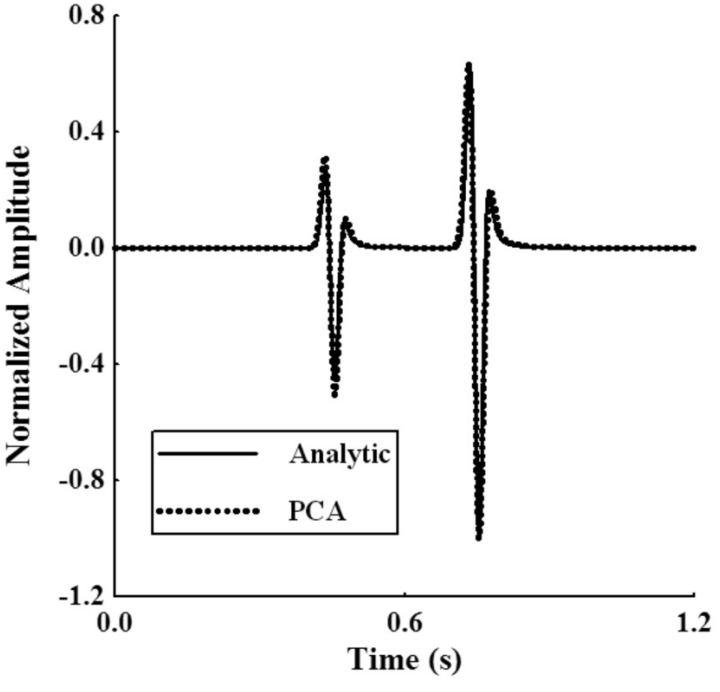

Fig. 9. The waveform comparison between the PCA and the analytic solution with the dominant frequency of $f_0 = 40$ Hz on the medium grid ($\Delta x = \Delta z = 8$ m) for the elastic model.

WAVEFIELD SIMULATIONS

In this section, we demonstrate the performance of the PCA in the 2D acoustic and elastic models and compare it against that of the fourth-order LWC method (Dablain, 1986). All numerical experiments are implemented on a PC with 1 GB memory and 1.33 GHz CPU.

Elastic isotropic model

In this example, we choose the Lamé constants $\lambda = 2.75$ GPa and $\mu = 6.25$ GPa, the density $\rho = 2.1$ g/cm^3. The source wavelet, a Ricker wavelet described by eq. (22) at the peak frequency $f_0 = 25$ Hz, is located at the center of the computation domain. The spatial and time increments are $\Delta x = \Delta z = 60$ m and $\Delta t = 0.003$ s, respectively. The computational domain is $0 < x \leq 18$ km and $0 < z \leq 18$ km, which results in 301×301 grid points. A receiver R is located at (x,z) = (10.5 km, 11.1 km).

Fig. 10 are the three-component wave-field snapshots at t = 2.5 s generated by the PCA. We can see that the P- and SV-waves shown in the horizontal component u_1 (Fig. 10a) and vertical component u_3 (Fig. 10c) have no apparent dispersive noise even though coarse grids ($\Delta x = \Delta z = 60$ m) are

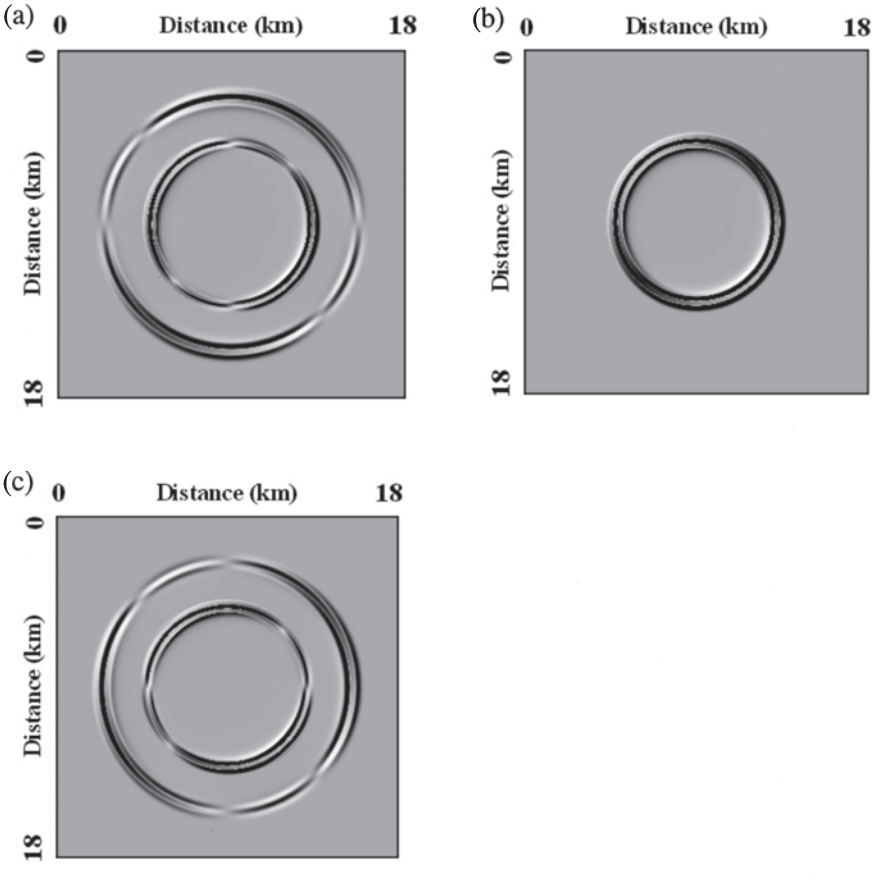

Fig. 10. Snapshots of seismic wave fields for three components at 2.5 sec in an elastic isotropic medium, generated by the PCA, for (a) u_1 component, (b) u_2 component, and (c) u_3 component.

used in the computation. It indicates that our method enables wave propagation to be simulated accurately in large-scale models using coarse computational grids.

Fig. 11 shows the waveforms of three components at the receiver R computed by the PCA (Fig. 11a) and the fourth-order LWC (Fig. 11b), respectively. Comparison between these two figures indicates that the PCA has almost no visible numerical dispersion, but the fourth-order LWC suffers from this numerical dispersion seriously.

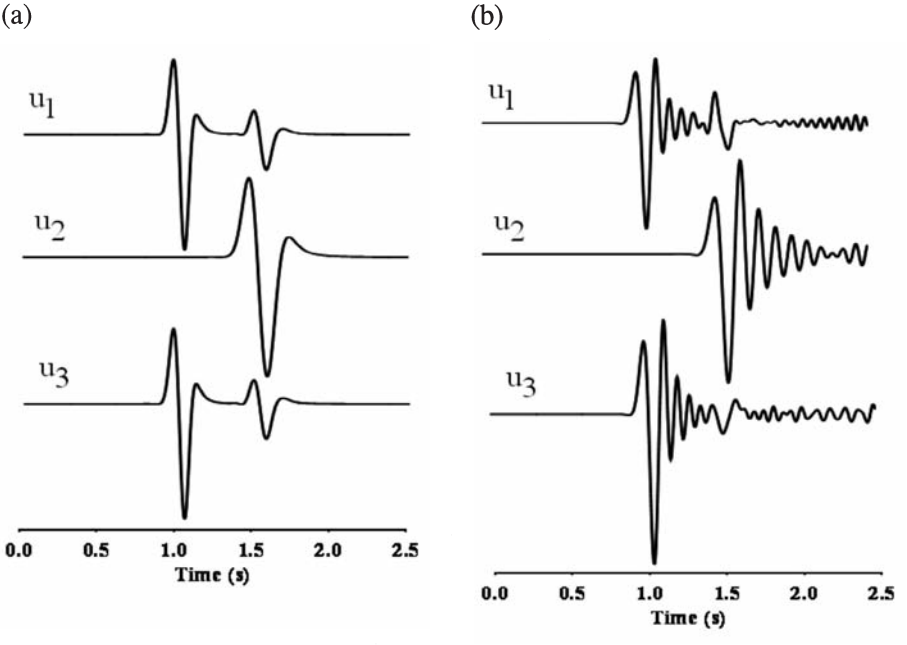

Fig. 11. Comparison of three-component waveforms for the elastic isotropic case, and the synthetic seismograms (a) and (b) are generated by the PCA and the fourth-order LWC method, respectively.

2D SEG/EAGE salt model

To further illustrate the applicability of the PCA in the heterogeneous medium, we test its performance using the 2D standard SEG/EAGE salt model shown in Fig. 12, which has strong velocity variations ranging from 1500 m/s to 4482 m/s. In this experiment, the numbers of grid points are 401 $\times$ 201, and we test two groups of spatial increments, $\Delta x = \Delta z = 20$ m and $\Delta x = \Delta z = 40$ m. The Ricker wavelet source formulated in eq. (22) with a peak frequency of $f_0 = 15$ Hz is located at the surface of the earth model.

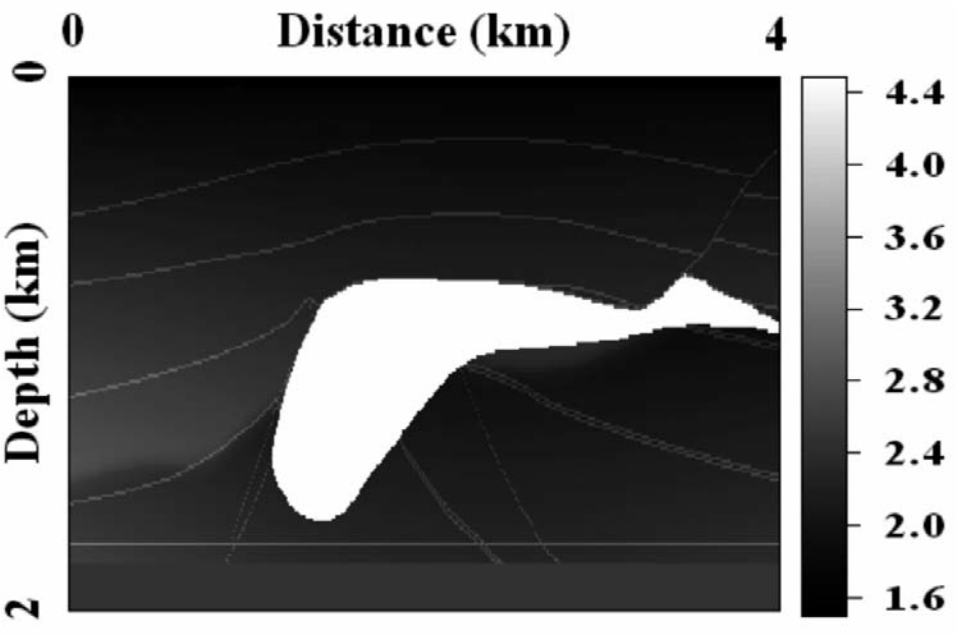

Fig. 12. SEG/EAGE salt model with the minimum acoustic velocity of 1500 m/s and maximum velocity of 4482 m/s.

Fig. 13 shows synthetic seismograms computed using the PCA which are respectively 4 second (Fig. 13a) and 8 second long (Fig. 13b). In the computation, we use free-surface boundary condition and apply the second-order absorbing boundary condition proposed by Yang et al., (2002). We can see that the synthetic seismic records for both fine and coarse grids are clearly free of numerical dispersion, which demonstrates the effectiveness of the PCA in numerical simulation in the complex heterogeneous medium.

CONCLUSIONS AND DISCUSSION

We suggest an explicit predictor-corrector algorithm (PCA) by using the implicit Runge-Kutta method to solve acoustic and elastic wave equations. We first transform the wave equation into an ordinary differential equation (ODE) system, then we use an implicit Runge-Kutta method associated with the predictor-corrector method to solve the ODE system by using the NAD operator to approximate the high-order spatial derivatives included in the ODE system. In other words, the time derivatives are approximated via the explicit predictor-corrector algorithm and the high-order space derivatives are calculated

(a)

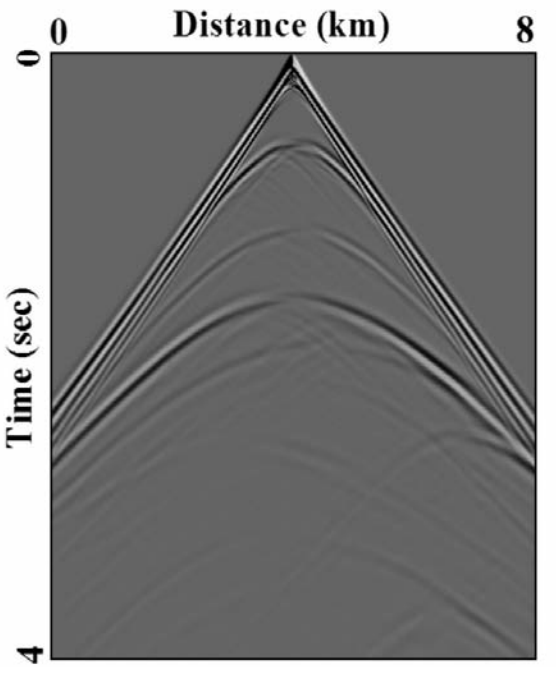

(b)

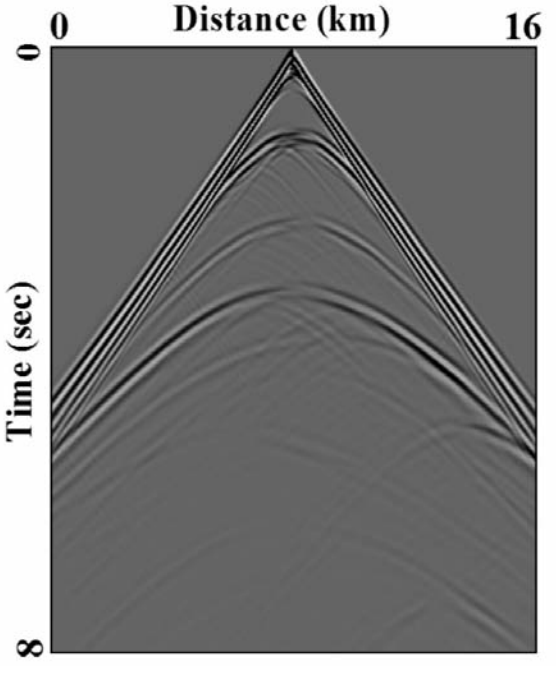

Fig. 13. Synthetic seismograms for the SEG/EAGE salt model generated by the PCA from time t = 0 to t = 4 s on a fine grid ($\Delta x = \Delta z = 20$ m) (a) and from time t = 0 to t = 8 s on the coarse grid ($\Delta x = \Delta z = 40$ m) (b).

using the multivariable interpolation approximation. On the basis of such a structure, we have to first convert these high-order time derivatives to the spatial derivatives, which is similar to the high-order FD or so-called LWC methods (Lax and Wendroff, 1964; Dablain, 1986). However, in approximating the high-order spatial derivatives the PCA is different from these high-order FD, LWC, and staggered-grid methods stated previously that only use the wave displacement at some grid points to approximate the high-order spatial derivatives or directly discretizing the original wave equation. This PCA uses simultaneously the wave displacement-, velocity- and their gradient fields to restructure the wave fields [see formulae (A-1) to (A-7)]. In other words, when determining these high-order spatial derivatives included in eq. (5), the PCA uses not only the values of the displacement **u** and the particle velocity **w** at the mesh point (i,j) and its neighboring gridpoints, but also the values of the gradients of the displacement **u** and particle velocity **w**. Based on such a structure, the PCA retains more wavefield information included in the displacement function, the particle velocity, and their gradients. As a result, the PCA can effectively suppress the numerical dispersion and source-generated noises caused by discretizing the wave equations when too-coarse grids are used or models have large velocity contrasts between adjacent layers. And the PCA has higher spatial accuracy though it only uses a local difference operator that three gridpoints are used in a spatial direction.

Theoretical error analysis shows the PCA is fourth-order accuracy in space and second-order accuracy in time, and its numerical convergence rate defined by the L^{∞}-norm (e.g., Dumbser and Köser, 2006) is about three. Comparison between the numerical results computed by the PCA and the analytical solution shows that the PCA is very effective in suppressing the numerical dispersion in both acoustic and elastic cases (see Figs. 5a, 6, 8 and 9). Both the numerical dispersion analysis and the wave-field simulation results show that the numerical dispersion error of the PCA is smaller than those of the SG scheme (Luo et al., 1990;Moczo et al., 2000) and the high-order LWC methods such as the fourth-order, eighth-order, and tenth-order LWC methods (Dablain, 1986) when the Courant number $\alpha \leq 0.5$.

Even though the PCA needs more central processing unit (CPU) time to compute the $\tilde{\mathbf{v}}^{n+1}$ at the (n+1)-th time step from $\tilde{\mathbf{v}}^{n}$ than those of the fourth-order LWC and the fourth-order SG method which is because the PCA needs more matrixes and the number of instructions for each time iteration, it allows much coarser grids to obtain the similar accuracy result as the other two methods on finer grids. As a result, the PCA is more efficient in overall computation and memory usage compared to the fourth-order LWC and the fourth-order SG method as shown in the numerical dispersion and efficiency section.

The PCA can be used for different applications in the large-scale wave field simulations, reverse time migration, and waveform inversion, etc, for its effectiveness in seismic simulation including solving the acoustic and elastic wave equations. Meanwhile, the PCA not only computes the displacement **u** and the particle velocity **w**, but also explicitly compute the gradients of the two wave-fields, so it can be easily extended to two-phase porous medium cases.

ACKNOWLEDGEMENTS

This work was supported by the National Science Fund for Distinguished Young Scholars of China (Grant No. 40725012) and the National Natural Science Foundation of China (Grant No. 41074073).

REFERENCES

Aki, K. and Richards, P.G., 1980. Quantitative Seismology: Theory and Methods. W.H. Freeman & Co., San Francisco.

Alford, R.M., Kelly, K.R. and Boore, D.M., 1974. Accuracy of finite-difference modeling of the acoustic wave equation. Geophysics, 39: 834-842.

Cockburn, B. and Shu, C.W., 1998. The Runge-Kutta discontinuous Galerkin method for conservation laws V: multidimensional systems. J. Computat. Phys., 141: 199-224.

Cockburn, B. and Shu C.W., 1989. TVB Runge-Kutta local projection discontinuous Galerkin finite element method for scalar conservation laws II: general framework. Mathemat. Computat., 52: 411-435.

Dablain, M.A., 1986. The application of high-order differencing to the scalar wave equation. Geophysics, 51: 54-66.

Dumbser, M. and Köser, M., 2006. An arbitrary high order discontinuous Galerkin method for elastic waves on unstructured meshes-II. The three-dimensional isotropic case. Geophys. J. Internat., 167: 316-336.

Eriksson, K. and Johnson, C., 1991. Adaptive finite element methods for parabolic problems: A linear model problem. SIAM J. Numer. Anal., 28: 43-77.

Fei, T. and Larner, K., 1995. Elimination of numerical dispersion in finite-difference modeling and migration by flux-corrected transport. Geophysics, 60: 1830-1842.

Fornberg, B., 1990. High-order finite differences and pseudo-spectral method on staggered grids. SIAM J. Numer. Anal., 27: 904-918.

Guan, Z. and Lu, J.F., 2006. Numerical methods. Tsinghua University Press, Beijing.

Hairer, E., Nørsett, S.P. and Wanner, G., 1993. Solving Ordinary Differential Equations I: Nonstiff Problems. Springer-Verlag, Berlin Heidelberg.

Johnson, C., 1990. Adaptive finite element methods for diffusion and convection problem. Comput. Meth. Appl. Mechan. Engin., 82: 301-322.

Köser, M. and Dumbser, M., 2006. An arbitrary high order discontinuous Galerkin method for elastic waves on unstructured meshes I: the two-dimensional isotropic case with external source terms. Geophys. J. Internat., 166: 855-877.

Komatitsch, D. and Vilotte, J.P., 1998. The Spectral Element method: an efficient tool to simulate the seismic response of 2D and 3D geological structures. Bull. Seismol. Soc. Am., 88: 368-392.

Komatitsch, D., Barnes, C. and Tromp, J., 2000. Simulation of anisotropic wave propagation based upon a spectral-element method. Geophysics, 65: 1251-1260.

Konddoh, Y., Hosaka, Y. and Ishii, K., 1994. Kernel optimum nearly analytical discretization algorithm applied to parabolic and hyperbolic equations. Comput. Mathem. Appl., 27: 59-90.

Kosloff, D. and Baysal, E., 1982. Forward modeling by a Fourier method. Geophysics, 47: 1402-1412.

Lax, P.D. and Wendroff, B., 1964. Difference schemes for hyperbolic equations with high order of accuracy. Communic. Pure Appl. Mathemat., 17: 381-398.

Lele, S.K., 1992. Compact finite difference scheme with spectral-like resolution. J. Computat. Phys., 103: 16-42.

Levander, A., 1988. Fourth-order finite-difference P-SV seismograms. Geophysics, 53: 1425-1436.

Luo, Y. and Schuster, G., 1990. Parsimonious staggered grid finite-differencing of the wave equation. Geophys. Res. Lett., 17: 155-158.

Moczo, P., Kristek, J. and Halada. L., 2000. 3D fourth-order staggered-grid finite-difference schemes: stability and grid dispersion. Bull. Seismol. Soc. Am., 90: 587-603.

Richtmeyer, R.D. and Morton, K.W., 1967. Difference Methods for Initial Value Problems. Interscience, New York.

Sei, A. and Symes, W., 1994. Dispersion analysis of numerical wave propagation and its computational consequences. J. Scientif. Comput., 10: 1-27.

Shu, C.W., 1988. Total-variation-diminishing time discretizations. SIAM J. Scientif. Statist. Comput., 9: 1073-1084.

Shu, C.W. and Osher, S., 1988. Efficient implementation of essentially non-oscillatory shock capturing schemes. J. Computat. Phys., 77: 439-471.

Takeuchi, N. and Geller, R.J., 2000. Optimally accurate second order time-domain finite difference scheme for computing synthetic seismograms in 2-D and 3-D media. Phys. Earth Planet. Inter., 119: 99-131.

Turner, M.J., Clough, R.W., Martin, H.C. and Topp, L.J., 1956. Stiffness and deflection analysis of complex structures. J. Aeronaut. Sci., 23: 805-823.

Virieux, J., 1984. SH-wave propagation in heterogeneous media: velocity stress finite-difference method. Geophysics, 49: 1933-1957.

Virieux, J., 1986. P-SV wave propagation in heterogeneous medium: Velocity-stress finite-difference method. Geophysics, 51: 889-901.

Wang, S.Q., Yang, D.H. and Yang, K.D., 2002. Compact finite difference scheme for elastic equations. J. Tsinghua Univ. Sci. Tech., 42: 1128-1131. (in Chinese)

Whiteman, J.R., 1975. A Bibliography for Finite Elements. Academic Press, New York.

Yang, D.H., Chen, S. and Li, J.Z., 2007. A Runge-Kutta method using high-order interpolation approximation for solving 2D acoustic and elastic wave equations. J. Seismic Explor., 16: 331-353.

Yang., D.H., Liu, E. and Zhang, Z.J., 2008. Evaluation of the u-W finite element method in anisotropic porous media. J. Seismic Explor., 17: 273-299.

Yang, D.H., Liu, E., Zhang, Z.J. and Teng, J., 2002. Finite-difference modeling in two-dimensional anisotropic media using a flux-corrected transport technique. Geophys. J. Internat., 148: 320-328.

Yang, D.H., Peng, J.M., Lu, M. and Terlaky, T., 2006. Optimal nearly analytic discrete approximation to the scalar wave equation. Bull. Seismol. Soc. Am., 96: 1114-1130.

Yang, D.H., Teng, J.W., Zhang, Z.J. and Liu, E., 2003. A nearly-analytic discrete method for acoustic and elastic wave equations in anisotropic media. Bull. Seismol. Soc. Am., 93: 882-890.

Yang, D.H., Wang, N., Chen, S. and Song, G.J., 2009. An explicit method based on the implicit Runge-Kutta algorithm for solving the wave equations. Bull. Seismol. Soc. Am., 99: 3340-3354.

Zahradnik, J., Moczo, P. and Hron, T., 1993. Testing four elastic finite-difference schemes for behavior at discontinuities. Bull. Seismol. Soc. Am., 83: 107-129.

Zhang, Z.J., Wang, G.J. and Harris, J.M., 1999. Multi-component wave-field simulation in viscous extensively dilatancy anisotropic media. Phys. Earth Planet. Inter., 114: 25-38.

Zheng, H.S., Zhang, Z.J. and Liu, E.R., 2006. Non-linear seismic wave propagation in anisotropic media using the flux-corrected transport technique. Geophys. J. Internat., 165: 943-956.

APPENDIX A

APPROXIMATIONS OF THE SPATIAL HIGH-ORDER DERIVATIVES

The explicit PCA needs to evaluate the high-order spatial derivatives included in eq. (5) or eqs. (6)-(11) and (13). Following Konddoh et al. (1994) and Yang et al. (2006), we compute them using a multi-variable high-order interpolation method. For convenience, we present the approximation formulae used in the PCA as follows

$$\partial_{2x}\mathbf{v}^n_{i,j} = (2/\Delta x^2)\delta_x^2\mathbf{v}^n_{i,j} - (1/2\Delta x)(E_x^1 - E_x^{-1})\partial_x\mathbf{v}^n_{i,j} \quad , \tag{A-1}$$

$$\partial_{2z}\mathbf{v}^n_{i,j} = (2/\Delta z^2)\delta_z^2\mathbf{v}^n_{i,j} - (1/2\Delta z)(E_z^1 - E_z^{-1})\partial_z\mathbf{v}^n_{i,j} \quad , \tag{A-2}$$

$$\begin{aligned}\partial_{xz}\mathbf{v}^n_{i,j} = {} & (1/2\Delta x)(E_x^1 - E_x^{-1})\partial_z\mathbf{v}^n_{i,j} + (1/2\Delta z)(E_z^1 - E_z^{-1})\partial_x\mathbf{v}^n_{i,j} \\ & - (1/4\Delta x\Delta z)(E_x^1E_z^1 - E_x^1E_z^{-1} - E_x^{-1}E_z^1 + E_x^{-1}E_z^{-1})\mathbf{v}^n_{i,j} \quad ,\end{aligned} \tag{A-3}$$

$$\begin{aligned}\partial_{3x}\mathbf{v}^n_{i,j} = {} & (15/2\Delta x^3)(E_x^1 - E_x^{-1})\mathbf{v}^n_{i,j} \\ & - (3/2\Delta x^2)(E_x^1 + 8I + E_x^{-1})\partial_x\mathbf{v}^n_{i,j} \quad ,\end{aligned} \tag{A-4}$$

$$\begin{aligned}\partial_{3z}\mathbf{v}^n_{i,j} = {} & (15/2\Delta z^3)(E_z^1 - E_z^{-1})\mathbf{v}^n_{i,j} \\ & - (3/2\Delta z^2)(E_z^1 + 8I + E_z^{-1})\partial_z\mathbf{v}^n_{i,j} \quad ,\end{aligned} \tag{A-5}$$

$$\begin{aligned}\partial_{2xz}\mathbf{v}^n_{i,j} = {} & (1/4\Delta x^2\Delta z) \\ & \times (5E_x^1E_z^1 - 5E_x^{-1}E_z^{-1} + E_x^1E_z^{-1} - E_x^{-1}E_z^1 - 4E_z^1 + 4E_z^{-1} - 6E_x^1 + 6E_x^{-1})\mathbf{v}^n_{i,j} \\ & + (1/2\Delta x\Delta z) \\ & \times (-E_x^1E_z^1 - E_x^{-1}E_z^{-1} + E_x^1 + E_x^{-1} - 2\delta_z^2)\partial_x\mathbf{v}^n_{i,j} + (1/\Delta x^2)\delta_x^2(\partial_z\mathbf{v}^n_{i,j}) \quad ,\end{aligned} \tag{A-6}$$

$$\begin{aligned}\partial_{x2z}\mathbf{v}^n_{i,j} = {} & (1/4\Delta x^2\Delta z) \\ & \times (5E_x^1E_z^1 - 5E_x^{-1}E_z^{-1} - E_x^1E_z^{-1} + E_x^{-1}E_z^1 - 4E_x^1 + 4E_x^{-1} - 6E_z^1 + 6E_z^{-1})\mathbf{v}^n_{i,j} \\ & + (1/2\Delta x\Delta z) \\ & \times (-E_x^1E_z^1 - E_x^{-1}E_z^{-1} + E_z^1 + E_z^{-1} - 2\delta_x^2)\partial_z\mathbf{v}^n_{i,j} + (1/\Delta z^2)\delta_z^2(\partial_x\mathbf{v}^n_{i,j}) \quad ,\end{aligned} \tag{A-7}$$

where the vector $\mathbf{v}$ is defined by $\mathbf{v} = (\mathbf{u},\mathbf{w})^T$, where $\mathbf{u}$ and $\mathbf{w}$ are respectively the wave field displacement and particle-velocity. The symbols $\mathbf{v}^n_{i,j}$, $\partial_x\mathbf{v}^n_{i,j}$, $\partial_z\mathbf{v}^n_{i,j}$ and $\partial_{mxkz}\mathbf{v}^n_{i,j}$ denote $\mathbf{v}(i\Delta x,j\Delta z,n\Delta t)$, $(\partial/\partial x)\mathbf{v}(i\Delta x,j\Delta z,n\Delta t)$, $(\partial/\partial z)\mathbf{v}(i\Delta x,j\Delta z,n\Delta t)$ and $(\partial^{m+k}\mathbf{v}/\partial x^m\partial z^k)^n_{i,j}$, respectively. The operators in the z-direction, involved in eqs. (A-1) - (A-7), are $\delta_z^2\mathbf{v}^n_{i,j} = \mathbf{v}^n_{i,j+1} - 2\mathbf{v}^n_{i,j} + \mathbf{v}^n_{i,j-1}$, $E_z^1\mathbf{v}^n_{i,j} = \mathbf{v}^n_{i,j+1}$, and $E_z^{-1}\mathbf{v}^n_{i,j} = \mathbf{v}^n_{i,j-1}$. The operators δ_x^2, E_x^1 and E_x^{-1} in the x-direction can be similarly defined.

APPENDIX B

DERIVATION OF THE STABILITY CRITERIA

1D Homogeneous Case

These formulae (A-1) and (A-4) for the 1D case can be degenerated into the following form,

$$\partial_{2x}\mathbf{v}^n_j = (2/\Delta x^2)\delta_x^2\mathbf{v}^n_j - (1/2\Delta x)(E_x^1 - E_x^{-1})\partial_x\mathbf{v}^n_j \quad , \tag{B-1}$$

$$\partial_{3x}\mathbf{v}^n_j = (15/2\Delta x^3)(E_x^1 - E_x^{-1})\mathbf{v}^n_j - (3/2\Delta x^2)(E_x^1 + 8I + E_x^{-1})\partial_x\mathbf{v}^n_j \quad , \tag{B-2}$$

where $\mathbf{v}^n_j = \mathbf{v}(j\Delta x,n\Delta t)$, $\delta_x^2\mathbf{v}^n_j = \mathbf{v}^n_{j+1} - 2\mathbf{v}^n_j + \mathbf{v}^n_{j-1}$, $E_x^1\mathbf{v}^n_j = \mathbf{v}^n_{j+1}$, and $E_x^{-1}\mathbf{v}^n_j = \mathbf{v}^n_{j-1}$.

To obtain the stability condition of the PCA, we consider the harmonic solution of eq. (6) for the 1D case. Substituting the following solution

$$\tilde{\mathbf{v}}^n_j = \begin{pmatrix} \mathbf{u}^n \\ \mathbf{w}^n \\ \partial_x\mathbf{u}^n \\ \partial_x\mathbf{w}^n \end{pmatrix} \exp[i(kjh)] \quad , \tag{B-3}$$

and the formulae (B-1) and (B-2) into eqs. (6) - (11) and (13), we can obtain the following equation

$$\tilde{\mathbf{v}}^{n+1} = \mathbf{G}\tilde{\mathbf{v}}^n \quad , \tag{B-4}$$

where $\mathbf{G}$ is the amplification matrix.

Let $\mathbf{G}^*$ denote the conjugate transpose matrix of $\mathbf{G}$. Following the Fourier analysis methods (Richtmeyer and Morton, 1967; Guan and Lu, 2006), we know that the PCA with the amplification matrix $\mathbf{G}$ is stable if the spectral radius $\rho(\mathbf{G}^*\cdot\mathbf{G})$ of $\mathbf{G}^*\cdot\mathbf{G}$ satisfies $\rho(\mathbf{G}^*\cdot\mathbf{G}) \leq 1$. So from the condition of $\rho(\mathbf{G}^*\cdot\mathbf{G}) \leq 1$, we can obtain the stability condition

$$\alpha \leq \alpha_{max} \leq 0.626 \quad , \tag{B-5}$$

or

$$\Delta t \leq \alpha_{max}(\Delta x/c_0) \approx 0.626(\Delta x/c_0) \quad , \tag{B-6}$$

where α_{max} denotes the maximum Courant number that keeps the PCA computational stable.

2D Homogeneous Case

For a 2D problem, we consider the case when $\Delta x = \Delta z = h$. Then, following the same analysis as in the 1D case above, we can obtain the following stability condition for the 2D case

$$\Delta t \leq \alpha_{max}(h/c_0) \approx 0.556(h/c_0) \quad . \tag{B-7}$$

APPENDIX C

DERIVATION OF THE NUMERICAL DISPERSION RELATION

1D Homogeneous Case

To investigate the numerical dispersion error of the PCA, we derive its numerical dispersion relation for the 1D case. Following the dispersion analysis methods presented in Dablain (1986) and Yang et al. (2006), we consider the harmonic solution of eq. (6) and substitute the solution for the 1D case

$$\tilde{\mathbf{v}}_j^n = \begin{pmatrix} \mathbf{u}_0 \\ \mathbf{w}_0 \\ \partial_x \mathbf{u}_0 \\ \partial_x \mathbf{w}_0 \end{pmatrix} \exp[i(\omega_{num} n\Delta t + kjh)] \quad , \tag{C-1}$$

into eqs. (6)-(11) and (13) with relations (B-1) and (B-2) to obtain the following dispersion equation

$$\mathrm{Det}(\mathbf{M}) = 0 \quad . \tag{C-2}$$

Due to the complexity of the matrix **M**, we omit its detail expressions.

From the dispersion relation (C-2), we can obtain the ratio of the numerical velocity to the phase velocity c_0 as follows

$$R = c_{num}/c_0 = \omega_{num}\Delta t/\alpha\theta = \gamma/\alpha\theta \quad , \tag{C-3}$$

where α is the Courant number, $\theta = kh$, in which k is the wave number and h $= \Delta x$ and $\gamma\ \omega_{num}\Delta t$ satisfies the dispersion eq. (C-2).

2D Homogeneous Case

For the 2D case, we derive the dispersion equation of the PCA for the case of $\Delta x = \Delta z = h$. Considering the harmonic solution of eq. (6), we substitute the solution

$$\tilde{\mathbf{v}}^{n}_{j,l} = \begin{pmatrix} \mathbf{v}_0 \\ \partial_x \mathbf{v}_0 \\ \partial_z \mathbf{v}_0 \end{pmatrix} \exp\{i[\omega_{num} n\Delta t + (k\cos\upsilon)jh] + (k\cos\upsilon)lh\} \quad , \tag{C-4}$$

into eq. (6) with relations (A-1) to (A-7) to obtain the 2D dispersion equation, which includes the plane-wave propagation angle with respect to the x-axis as an independent variable υ. The detailed derivation of the dispersion equation for the 2D case is omitted here, and we only show the ratio of the numerical velocity to the phase velocity R ($R = c_{num}/c_0$) by solving the 2D dispersion equation. The dispersion curves of the PCA under Courant number 0.1 and 0.4 are shown in Fig. 2, and the dispersion relation curves of the SG method under the same Courant number are also shown for comparison.